

Axisymmetric withdrawal and inflow in a density-stratified container

By G. N. IVEY AND S. BLAKE

Research School of Earth Sciences, Australian National University,
GPO Box 4, Canberra, A.C.T. 2601

(Received 5 August 1984 and in revised form 15 May 1985)

The axisymmetric withdrawal of fluid from a linearly stratified container is studied over the full parameter range. When only buoyancy and inertia are important the flow in the withdrawal layer is influenced by a virtual control point and is not analogous to that observed in the two-dimensional withdrawal problem. Two further flow regimes are shown to exist in which viscous forces are important: one in which convection of species is important, and a second in which diffusion of species is important. Theoretical arguments and laboratory experiments are used to show that $S = (Q^2 N / \nu^3)^{1/2}$ is the appropriate flow parameter to differentiate between these possibilities. It is also argued that these results may be generalized to describe the features of several related flows: axisymmetric drawdown (or drawup) in withdrawal from a layered density structure, axisymmetric inflow into a linearly stratified environment and the axisymmetric spreading of density currents.

1. Introduction

The withdrawal of fluid from a density-stratified container (i.e. selective withdrawal) has long been a subject of interest as a management technique for the control of water quality in water supply reservoirs. Selective withdrawal, however, has a much wider application. Pumped sampling systems are often used by marine biologists, for example, to determine phytoplankton concentrations in stratified oceans or lakes (Fasham 1978), and the vertical scale of the sampling is of fundamental interest. On a larger scale the production of mixed magmas from active volcanoes is also a problem in selective withdrawal from the stratified magma chamber (Blake & Ivey 1985). In addition to the diverse applications of selective withdrawal, there is also a close analogy between withdrawal and inflow into a stratified fluid. Thus an understanding of the withdrawal process sheds considerable light on a range of inflow problems.

The majority of work to date has been in the study of two-dimensional selective withdrawal—the withdrawal of fluid from rectangular containers through a line sink. Imberger (1980) provides a comprehensive review of this work. He identifies three basic flow regimes, delineated by the transition parameter $R = F_2 Gr^{1/2}$ where the Froude number $F_2 = q/NL^2$ and the Grashof number $Gr = N^2 L^4 / \nu^2$. In this context, q is the discharge per unit width, N is the buoyancy frequency, ν is the kinematic viscosity and L is the horizontal distance from the sink to the upstream boundary.

The withdrawal layer may be assumed to be steady throughout the container when

it is steady at the upstream boundary (Imberger 1980), and at steady state the withdrawal-layer thickness δ is given by

$$\delta \sim \left(\frac{q}{N}\right)^{\frac{1}{2}} = LF^{\frac{1}{2}} \quad (R > 1), \quad (1a)$$

$$\delta \sim \left(\frac{\nu q L}{N^2}\right)^{\frac{1}{2}} = LGr^{-\frac{1}{2}}R^{\frac{1}{2}} \quad (Sc^{-\frac{1}{2}} < R < 1), \quad (1b)$$

$$\delta \sim (\nu D)^{\frac{1}{2}} \left(\frac{L}{N}\right)^{\frac{1}{2}} = LGr^{-\frac{1}{2}}Sc^{-\frac{1}{2}} \quad (R < Sc^{-\frac{1}{2}}), \quad (1c)$$

where the Schmidt number $Sc = \nu/D$ and D is the diffusivity of the stratifying species. In the present study δ is taken as the withdrawal-layer half-thickness: the vertical distance from the horizontal centreline of the induced horizontal velocity profile to the first zero-crossing of that velocity profile (see figure 2 for a definition sketch). The evolution of the flow to steady state and the characteristics of these three regimes at steady state are described in detail by Imberger, Thompson & Fandry (1976, hereinafter denoted by ITF).

In contrast, comparatively little work has been done on axisymmetric withdrawal. Both Lawrence (1980) and Spigel & Farrant (1984) have examined the withdrawal of fluid via a point sink from long rectangular containers in the regime where inertia and buoyancy forces are important. Their work is discussed in detail in §4 below. These authors point out that withdrawal structures in most water-supply reservoirs act as point sinks. The same is true of many other withdrawal configurations, such as the magma-chamber withdrawal problem. The axisymmetric withdrawal of fluid from a stratified container is thus of considerable practical interest.

Our purpose in the present work is to examine the axisymmetric withdrawal from a stratified fluid in a bounded container over the entire parameter range. The fluid will be assumed continuously stratified and the transport coefficients ν and D constant in value. The effect of variable viscosity is discussed in Blake & Ivey (1985). We also follow ITF by neglecting the effects of the sidewall boundary layers in order to focus on the dynamics of the withdrawal layer itself. The initial motion after commencing withdrawal is discussed in §2. The steady-state withdrawal layers, governed by either a balance between viscous and buoyancy forces or a balance between inertia and buoyancy forces, are discussed in §3. Section 4 presents the results of the laboratory experiments covering both regimes. Section 5 addresses the problem of withdrawal from a discontinuously stratified fluid. Section 6 discusses the analogy between these withdrawal configurations and the problem of axisymmetric inflow into stratified and homogeneous environments. Finally, §7 presents the conclusions from this study.

2. Initial motion

In studies of the withdrawal of fluid from stratified containers through a line sink, Pao & Kao (1974) and ITF have described the dynamics of the initial motion following the sudden initiation of withdrawal. Immediately after the sink is turned on, a nearly horizontal potential flow is created. This flow is then progressively modified by a discrete spectrum of planar shear waves that travel out from the sink against the induced uniform upstream velocity. As McEwan & Baines (1974) found, each shear wave front travels with a speed $c_n = NH/n\pi$, where n is the modal number

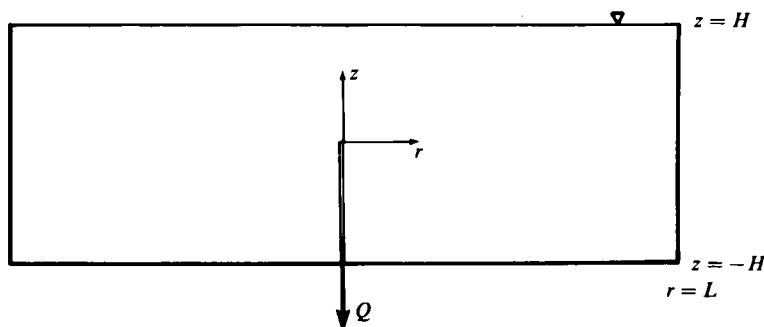


FIGURE 1. Definition sketch of configuration for axisymmetric withdrawal from a circular container

and H the depth, and has a frontal width $w_n = H(NT)^{1/2}/n$, where T is the time. The modification of the potential flow by these shear waves dominates the initial dynamics of the flow.

In the case of axisymmetric withdrawal through a point sink, a similar behaviour has been found. Following the sudden initiation of withdrawal through a point sink, Lawrence & Imberger (1979) and Lawrence (1980) demonstrated that a series of now cylindrical shear waves travel out from the sink. The induced velocity field in a semi-infinite domain is given by

$$\psi(r, z, t) = \frac{Q}{4\pi H} \left[z + \sum_{n=1}^{\infty} \frac{2}{n\pi} \sin\left(\frac{n\pi z}{H}\right) \frac{t}{[(tN)^2 - (n\pi r/H)^2]^{1/2}} \bar{H}\left(tN - \frac{n\pi r}{H}\right) \right], \quad (2)$$

where \bar{H} is the Heaviside step function.

We can generalize these results to the problem of axisymmetric withdrawal from the bounded container with the configuration shown in figure 1. Since the initial motion after turning on the sink is dominated by the presence of propagating shear waves, the correct non-dimensional variables to introduce are (see also ITF)

$$\begin{aligned} r' &= rH^{-1}, & z' &= zH^{-1}, & t' &= TN, & u' &= uQ^{-1}H^2, & w' &= wQ^{-1}H^2, \\ \rho' &= \rho(\rho_0 QN)^{-1}gH^2, & p' &= p(\rho_0 QN)^{-1}H, \end{aligned}$$

where the total density is decomposed as $\rho_t = \rho_0 + \rho_e(z) + \rho(r, z, t)$ and the buoyancy frequency $N^2 = -(g/\rho_0)d\rho_e/dz$ is a constant. In terms of these variables, the Boussinesq approximations to the equations of motion are (dropping the primes)

$$\frac{1}{r} \frac{\partial}{\partial r} (ru) + \frac{\partial w}{\partial z} = 0, \quad (3a)$$

$$\frac{\partial u}{\partial t} + A^{-3}F \left[u \frac{\partial u}{\partial r} + w \frac{\partial u}{\partial z} \right] = -\frac{\partial p}{\partial r} + \left(\frac{Sc}{A^4 Ra} \right)^{1/2} \left[\nabla^2 u - \frac{u}{r^2} \right], \quad (3b)$$

$$\frac{\partial w}{\partial t} + A^{-3}F \left[u \frac{\partial w}{\partial r} + w \frac{\partial w}{\partial z} \right] = -\frac{\partial p}{\partial z} + \rho + \left(\frac{Sc}{A^4 Ra} \right)^{1/2} \nabla^2 w, \quad (3c)$$

$$\frac{\partial \rho}{\partial t} + A^{-3}F \left[u \frac{\partial \rho}{\partial r} + w \frac{\partial \rho}{\partial z} \right] = -w + (ScA^4 Ra)^{-1/2} \nabla^2 \rho, \quad (3d)$$

where the aspect ratio $A = H/L$ and the Rayleigh number $Ra = N^2 L^4 / \nu D$.

Introducing the axisymmetric stream function, and taking the limit when the Froude number $F = Q/NL^3 \rightarrow 0$ and the Rayleigh number $Ra \rightarrow \infty$, these equations can be reduced to the linear inviscid non-diffusive equation for the axisymmetric stream function given by

$$\psi_{zztt} + \psi_{rrtt} - \frac{1}{r} \psi_{ritt} + \psi_{rr} - \frac{1}{r} \psi_r = 0. \quad (4)$$

This equation is to be solved subject to the boundary conditions for $t \geq 0$: (i) $\psi = (Ar)^2 - \frac{1}{2}$ on $z = 1$; (ii) $\psi = \frac{1}{2}$ on $z = -1$; (iii) $\psi = -\frac{1}{2} \operatorname{sgn} z$ on $r = 0$; (iv) $\psi = \frac{1}{2}$ on $Ar = 1$; and the initial conditions are (v) $\nabla^2 \psi = \nabla^2 \psi_t = 0$. In writing condition (i) we have assumed that the baroclinic and barotropic motions are separable.

Taking the Laplace transform of (4) yields the solution

$$\bar{\psi}(r, z, s) = \frac{(Ar)^2}{2s} + \frac{((Ar)^2 - 1)z}{2s} + \sum_{n=1}^{\infty} \frac{1}{(s^2 + 1)^{\frac{1}{2}}} \left[\frac{K_1(\lambda/A)}{I_1(\lambda/A)} r I_1(\lambda r) - r K_1(\lambda r) \right] \sin n\pi z,$$

where

$$\lambda = \frac{n\pi s}{(s^2 + 1)^{\frac{1}{2}}}.$$

Inverting for small time yields

$$\psi(r, z, t = 0^+) \sim \frac{1}{2}(Ar)^2 + \frac{1}{2}((Ar)^2 - 1)z + \sum_{n=1}^{\infty} \left[\frac{K_1(n\pi/A)}{I_1(n\pi/A)} r I_1(n\pi r) - r K_1(n\pi r) \right] \sin n\pi z. \quad (5)$$

Comparing the first two terms in (5) (the axisymmetric potential-flow solution) with the corresponding term in (2), it is clear that the effect of the endwall is to induce a more-rapid decrease of horizontal velocity with distance from the sink than the linear decay observed in the unbounded domain. In both cases, however, the solution consists of an initial potential flow, subsequently modified by a discrete spectrum of propagating shear waves, as in the two-dimensional problem.

In their detailed study of this problem ITF demonstrated that the shear waves were continually attenuated by diffusion of vorticity and mass and modified by convection induced by the previous waves. If the regime parameter R (see (1)) is greater than one, then convection dominates and waves will propagate out until the induced flow just balances their phase velocity. A balance between inertia and buoyancy prevails at steady state. Conversely, if R is less than one the authors demonstrated waves will propagate until they have decayed by viscous action. A balance between viscosity and buoyancy prevails at steady state.

Since the form of the initial behaviour is the same in both the line sink and axisymmetric withdrawal configurations, it is reasonable to anticipate that there should be a similarity in the long-time behaviour of the flows in the two configurations (this is confirmed by the experiments discussed in §4) – a similarity in that two basic steady-state axisymmetric withdrawal-layer configurations can develop: in the first a regime with a balance between buoyancy and viscous forces, and in the second a regime with a balance between buoyancy and inertial forces.

3. Axisymmetric withdrawal-layer structure

3.1. The viscous–buoyancy withdrawal layer

Let us consider the development of the flow beyond the initial motion in the case where we expect buoyancy and viscous forces to be important. Further, let us consider

only fluids with $Sc = \nu/D = O(1)$ for the moment. As Imberger (1980) notes, the evolution to steady state is achieved by the viscous dissipation of the shear waves, and the n th wave will have dissipated in time $T \sim \lambda_n^2/\nu$, where the vertical wavelength $\lambda_n \sim H/n$ and the wave speed $c_n \sim N\lambda_n$. Whether the shear fronts are planar or cylindrical in form will make no difference to this estimated timescale. A withdrawal-layer structure will have formed when a wave is first dissipated at the upstream boundary of the tank, and the non-dimensionalized layer thickness δ for this lengthscale L is

$$\frac{\delta}{L} \sim \frac{\lambda_n}{L} \sim Gr^{-\frac{1}{2}} \quad \text{in time } T \sim N^{-1}Gr^{\frac{1}{2}}.$$

The correct non-dimensional variables for times of this magnitude are then

$$\begin{aligned} r' &= rL^{-1}, \quad z' = zL^{-1}Gr^{\frac{1}{2}}, \quad t' = TNGr^{-\frac{1}{2}}, \quad u' = uQ^{-1}L^2Gr^{-\frac{1}{2}}, \quad w' = WQ^{-1}L^2, \\ \rho' &= \rho(\rho_0\nu Q)^{-1}gL^4Gr^{-\frac{1}{2}}, \quad p' = p'(\rho_0\nu Q)^{-1}L^3Gr^{-\frac{1}{2}}. \end{aligned}$$

In terms of these new variables, the equations of motion may now be written (dropping the primes)

$$\frac{\partial u}{\partial t} + FGr^{\frac{1}{2}} \left[u \frac{\partial u}{\partial r} + w \frac{\partial u}{\partial z} \right] = -\frac{\partial p}{\partial r} + Gr^{-\frac{1}{2}} \left[\frac{\partial}{\partial r} \left(\frac{1}{r} \frac{\partial}{\partial r} (ru) \right) \right] + \frac{\partial^2 u}{\partial z^2}, \quad (6a)$$

$$Gr^{-\frac{1}{2}} \frac{\partial w}{\partial t} + F \left[u \frac{\partial w}{\partial r} + w \frac{\partial w}{\partial z} \right] = -\frac{\partial p}{\partial z} - \rho + Gr^{-\frac{1}{2}} \left[\frac{1}{r} \frac{\partial}{\partial r} \left(r \frac{\partial w}{\partial r} \right) \right] + Gr^{-\frac{1}{2}} \frac{\partial^2 w}{\partial z^2}, \quad (6b)$$

$$\frac{\partial \rho}{\partial t} + FGr^{\frac{1}{2}} \left[u \frac{\partial \rho}{\partial r} + w \frac{\partial \rho}{\partial z} \right] = -w + Sc^{-1}Gr^{-\frac{1}{2}} \left[\frac{1}{r} \frac{\partial}{\partial r} \left(r \frac{\partial \rho}{\partial r} \right) \right] + Sc^{-1} \frac{\partial^2 \rho}{\partial z^2}. \quad (6c)$$

Introducing the axisymmetric stream function, considering the case where $R = FGr^{\frac{1}{2}} \ll 1$, and retaining terms correct to $O(Gr^{-\frac{1}{2}})$, these equations may be reduced to the single equation

$$\begin{aligned} \frac{1}{rSc} \psi_{zzzzz} - \frac{1+Sc}{rSc} \psi_{zzzt} + \frac{1}{r} \psi_{zztt} - \left(\frac{\psi_r}{r} \right)_r \\ + Gr^{-\frac{1}{2}} \left[\frac{1}{r} \psi_{rrt} + \frac{3}{Sc} \left(\frac{1}{r} \psi_{zzzz} \right)_r - \frac{1}{rSc} \psi_{zzrrt} - \frac{1}{Sc} \left(\frac{1}{r} \psi_{zzrt} \right)_r - 2 \left(\frac{1}{r} \psi_{zzrt} \right)_r \right] = 0. \quad (7) \end{aligned}$$

Equation (7) is directly analogous to (15) in ITF. As in the two-dimensional case, the flow ultimately reaches a steady state in which both viscosity and the diffusivity of the stratifying species are important. That is, in the limit of large Gr , (6) reduces to

$$\frac{\partial \rho}{\partial r} = \frac{\partial^3 u}{\partial z^3}, \quad w = \frac{\partial^2 \rho}{\partial z^2}.$$

In dimensional form this balance yields a steady-state withdrawal-layer scale $\delta \sim LGr^{-\frac{1}{2}}Sc^{-\frac{1}{2}}$ – found by Koh (1966). The time for this final steady state to appear is $T \sim N^{-1}Gr^{\frac{1}{2}}Sc^{\frac{1}{2}}$ (see below).

While this is the behaviour for fluids with Sc (or Pr) = $O(1)$, our interest here is for fluids with $Sc \gg 1$ – as found in the laboratory, with salt stratification, for example, and in the magma-chamber withdrawal problem (Blake & Ivey 1985) which originally motivated this study. In the limit of large Sc and Gr , (7) simplifies to

$$\frac{1}{r} \psi_{zztt} - \frac{1}{r} \psi_{zzzt} - \left(\frac{\psi_r}{r} \right)_r = 0.$$

As ITF point out, the first term is only important for $t = O(1)$. For $t > 1$ the remaining terms admit a similarity solution of the form

$$\psi = \psi(\eta), \quad \text{where } \eta = zt^{\frac{1}{2}}r^{-\frac{1}{2}}$$

Substituting this similarity form back into (6), then in the limit of large Grashof number we obtain a pair of equations for momentum and species conservation respectively of the form

$$\frac{1}{2} \frac{r}{t^{\frac{3}{2}}} (\psi'' + \frac{1}{2}\eta\psi''') - \frac{R}{r^{\frac{3}{2}}t^{\frac{3}{2}}} 3\psi'\psi'' = -\rho + \frac{1}{2}\eta\rho' + \psi''', \quad (8a)$$

$$\rho + \frac{1}{4}\eta\rho' + \frac{1}{2}\eta\psi' - \frac{2Rt^{\frac{1}{2}}}{r^{\frac{3}{2}}} \rho\psi' = \frac{1}{Sc} \frac{t^{\frac{1}{2}}}{r} \rho'' \quad (8b)$$

(where primes refer to differentiation with respect to η).

These equations describe the evolution of the withdrawal layer in a bounded container (with $r = O(1)$) where $R = FGt^{\frac{1}{2}} < 1$, when Sc is large and when $t > 1$. It is evident from the species equation (8b) that the similarity form above will break down when either the species-convection or diffusion terms grow to the same order of magnitude as the convection of the background gradient.

From (8b) it is clear, first, that species convection will become important in time $t \sim R^{-\frac{4}{3}}$ or, dimensionally, in time $T \sim N^{-1}Gr^{\frac{1}{3}}R^{-\frac{4}{3}}$. This timescale for self-induced convection to become important corresponds to the time it takes to fall one withdrawal-layer thickness (i.e. $T \sim L^2\delta/Q$), which yields the withdrawal-layer scale

$$\delta \sim LGr^{-\frac{1}{3}}R^{\frac{1}{3}} = \left(\frac{\nu Q}{N^2}\right)^{\frac{1}{3}}. \quad (9a)$$

Unlike its two-dimensional counterpart (1b), the withdrawal-layer thickness is now *independent* of distance from the sink.

Secondly, it is evident from (8b) that diffusion of species will become important in time $t \sim Sc^{\frac{2}{3}}$ or, dimensionally, in time $T \sim N^{-1}Gr^{\frac{1}{3}}Sc^{\frac{2}{3}}$. This timescale represents the time it takes for diffusion to act over one withdrawal-layer scale (i.e. $T \sim \delta^2/D$), which yields the withdrawal-layer scale

$$\delta \sim LGr^{-\frac{1}{3}}Pr^{-\frac{1}{3}} = \frac{(\nu D)^{\frac{1}{3}}L^{\frac{1}{3}}}{N^{\frac{1}{3}}}, \quad (9b)$$

i.e. the same structure as the final steady state for fluids with $Sc \sim 1$.

Finally, we note that species convection will become important before species diffusion if $R^{-\frac{4}{3}} < Sc^{\frac{2}{3}}$ or $R > Sc^{-\frac{4}{3}}$. In summary, for the case $R = FGt^{\frac{1}{2}} < 1$ (i.e. $L > Q^{\frac{1}{3}}N^{-\frac{1}{3}}\nu^{-\frac{2}{3}}$) the initial viscous-buoyancy layer of thickness $\delta \sim LGr^{-\frac{1}{3}}$ will undergo secondary collapse for time $T > N^{-1}Gr^{\frac{1}{3}}$. If $Sc^{-\frac{4}{3}} < R < 1$ a viscous-convective withdrawal layer of thickness $\delta \sim (\nu Q/N^2)^{\frac{1}{3}}$ forms. Conversely, if $R < Sc^{-\frac{4}{3}}$ a viscous-diffusive withdrawal layer forms of thickness $\delta \sim (\nu D)^{\frac{1}{3}}L^{\frac{1}{3}}N^{-\frac{1}{3}}$. In the viscous regime the axisymmetric withdrawal layer thus behaves much like its two-dimensional counterpart. The major difference is in the viscous-convective regime, where in the two-dimensional case the withdrawal layer has a thickness that increases with distance upstream from the sink (equation (1b)), while in the axisymmetric case the withdrawal-layer thickness is constant (equation (9a)).

3.2. The inertial–buoyancy withdrawal layer

In this regime the temptation is to argue once again by analogy with the two-dimensional results. It is instructive to do this, but, as will become evident, the analogy between two- and three-dimensional flows now breaks down.

If viscosity is unimportant then in the two-dimensional case planar shear waves continue to propagate out from the sink until the flow velocity – induced by the previous waves – just balances their phase velocity. Smaller waves are swept out of the sink, and the local thickness of the withdrawal layer is exactly equal to the vertical wavelength of the highest-mode-number wave able to propagate upstream (ITF). While the propagating shear waves are cylindrical in the axisymmetric case, the same balance should prevail at steady state. A steady-state balance involving only inertia and buoyancy forces would then take the form

$$\frac{\partial}{\partial z} (\mathbf{u} \cdot \nabla \mathbf{u}) = -\frac{g}{\rho_0} \frac{\partial \rho}{\partial r}, \quad (10a)$$

$$\mathbf{u} \cdot \nabla \rho = -w \frac{d\rho_e}{dz}. \quad (10b)$$

Such a balance yields a withdrawal-layer scale of

$$\delta \sim \left(\frac{Q}{NL} \right)^{\frac{1}{2}} \sim LF^{\frac{1}{2}} \quad \text{in time } T \sim N^{-1} F^{-\frac{1}{2}}. \quad (10c)$$

Equation (10c) is analogous to (1a). Now, however, the balance in the axisymmetric case suggests an inertia–buoyancy layer which *decreases* in thickness with increasing distance from the sink. It is evident from (5) that the vertical wavenumber of the shear waves is independent of distance from the sink. Clearly then, a steady-state balance between the upstream propagation of shear waves and an induced downstream flow cannot possibly yield a withdrawal layer whose thickness decreases with increasing distance upstream, as suggested by (10). Indeed, an initial experiment by Lawrence & Imberger (1979) (see also Lawrence 1980), a more extensive set of experiments by Spigel & Farrant (1984) and our own laboratory experiments (§4) all indicate the withdrawal layer has a *constant* thickness of $\delta \sim (Q/N)^{\frac{1}{2}}$. This inconsistency may be resolved by considering the approach to steady state. Since the local thickness of the withdrawal layer is exactly equal to the wavelength of the highest-mode wave able to propagate to that station (ITF), then any factor that controls the upstream propagation of these waves will influence, in turn, the final steady-state structure.

Bryant & Wood (1976) pointed out that a point of virtual control exists in the flow field if the local value of the internal Froude number is unity. In the present context, since the phase speed of the shear waves $c_n \sim NH/n \sim N\lambda_n$, where λ_n is the vertical wavelength and equal to the withdrawal-layer thickness δ , the internal Froude number $F_1 \sim (Q/\delta r)/N\delta$. It is experimentally observed (see §4) that the steady-state withdrawal-layer thickness $\delta \sim (Q/N)^{\frac{1}{2}}$. With this observation, it is clear that $F_1 \sim 1$ at $r \sim (Q/N)^{\frac{1}{2}}$ – and this defines the location r_v of a point of virtual control. When a position of virtual control exists in the flow field, shear waves with vertical wavelength $\delta < (Q/N)^{\frac{1}{2}}$ are unable to propagate upstream beyond the position of virtual control. Consequently, the withdrawal layer upstream of the virtual control

point is unable to collapse *beyond* a thickness of order $(Q/N)^{\frac{1}{2}}$. The steady-state layer thickness is therefore

$$\delta \sim \left(\frac{Q}{N}\right)^{\frac{1}{2}} \quad \text{in time } T \sim \frac{L}{c} \sim N^{-\frac{1}{2}}Q^{-\frac{1}{2}}L. \quad (11)$$

While (9*a, b*) and (11) define three possible steady-state withdrawal layers, the transition between the inertial and viscous regimes is not clearly defined. One method of deriving a transition criterion is to consider a tank sufficiently long to include more than one flow regime and to ask at what point do the steady-state layer thicknesses for each regime match? It is easy to show that in the two-dimensional case this type of matching procedure yields a single transition criterion: the parameter R in (1). For $R > 1$ an inertia–buoyancy withdrawal layer is present; and if $R < 1$ then only viscous–buoyancy withdrawal layers can exist.

Following this approach, Lawrence & Imberger (1979) and Lawrence (1980) matched the observed axisymmetric inertial-layer thickness from (11), with the viscous-diffusive-layer thickness, from (9*b*), to obtain the transition parameter $Q/(\nu D)^{\frac{1}{2}}L$. If this parameter is much greater than one (i.e. $L < Q/(\nu D)^{\frac{1}{2}}$) then the flow is inertial and described by (11). Conversely, if $L > Q/(\nu D)^{\frac{1}{2}}$ the flow is viscous, and described by (9*b*). If we follow this procedure and take the ratio of the inertial-layer thickness in (11) to the viscous–convective layer thickness in (9*a*), we now obtain a different transition parameter, denoted here by S for future reference, of

$$S = \left(\frac{Q^2 N}{\nu^3}\right)^{\frac{1}{3}}. \quad (12)$$

In order to differentiate between these two transition criteria, consider a tank of sufficiently large radius that there is a region close to the sink where the flow is dominated by inertial forces, and at some point upstream we anticipate the flow will be slow enough that viscous forces will become important. A *necessary* condition for viscous forces to be important and inertia forces to be negligible is, from §3.1, that $R = FG\tau^{\frac{1}{2}} < 1$ or $L > L_v \sim Q^{\frac{1}{2}}N^{-\frac{1}{2}}\nu^{-\frac{1}{2}}$. This is not *sufficient*, however, to ensure viscous flow, since a second horizontal lengthscale, the position of the virtual point at $r_v \sim (Q/N)^{\frac{1}{2}}$, must also be considered. We note that the ratio $L_v/r_v = S^2$, as defined in (12), and thus the parameter S provides a convenient measure of the relative magnitude of *both* horizontal lengthscales of importance in governing the transition from inertial to viscous regimes in axisymmetric withdrawal.

If the ratio L_v/r_v is large then a virtual control point is present in the flow. Upstream of the potential-flow region adjacent to the sink there exists an inertial–buoyancy withdrawal layer of constant thickness $\delta \sim (Q/N)^{\frac{1}{2}}$. At distances upstream of $L > Q/(\nu D)^{\frac{1}{2}}$ diffusion of species becomes important, and the flow moves into a viscous–diffusive regime with thickness $\delta \sim (\nu D)^{\frac{1}{2}}L^{\frac{1}{2}}N^{-\frac{1}{2}}$. The layer thus continues to grow in thickness with increasing distance upstream. In this case, with S large, no viscous–convective regime is found in the flow field. Indeed, this lack of a physical transition to a viscous–convective regime is reflected in the fact that there is no lengthscale present in the definition of S in (12).

If the ratio L_v/r_v is small, on the other hand, there exists the possibility that viscous forces govern the flow *before* the virtual control point is reached. Effectively no virtual control point exists in the flow field. Upstream of the potential-flow region adjacent to the sink there exists a viscous–convective withdrawal layer of constant thickness $\delta \sim (\nu Q/N^2)^{\frac{1}{2}}$. At distances upstream of $L > Q^{\frac{1}{2}}\nu^{\frac{1}{2}}N^{-\frac{1}{2}}D^{-\frac{1}{2}}$ (i.e. $R = FG\tau^{\frac{1}{2}} < Sc^{-\frac{1}{2}}$)

Regime	Steady-state withdrawal-layer half-thickness δ and time T_s to steady state	Constant of proportionality	Source
	(a) $S > S_{crit}$		
(A) $S > S_{crit}$ and $S > (GrSc^{-2})^{1/3}$	$\delta = c_1 \left(\frac{Q}{N}\right)^{1/3}$	$c_1 = 0.66$	Lawrence & Imberger (1979)
	in $T_s \sim (N^{-1/3}Q^{-1/3}L)$	$c_1 = 0.81$ $c_1 = 0.66$ average $c_1 = 0.71$	Spigel & Farrant (1984) Present study (figure 4)
(B) $S > S_{crit}$ and $S < (GrSc^{-2})^{1/3}$	$\delta = c_2(\nu D)^{1/3} \left(\frac{L}{N}\right)^{1/3}$	$c_2 = 2.9$	Koh (1966)
	in $T_s \sim N^{-1}Gr^4Sc^3$		
	(b) $S < S_{crit}$		
(C) $S < S_{crit}$ and $S > (GrSc^{-2})^{1/3}$	$\delta = c_3 \left(\frac{\nu Q}{N^2}\right)^{1/3}$	$c_3 = 2.1$	Present study (figure 5)
	in $T_s \sim N^{-1}Gr^4Sc^{-6}$		
(D) $S < S_{crit}$ and $S < (GrSc^{-2})^{1/3}$	$\delta = c_2(\nu D)^{1/3} \left(\frac{L}{N}\right)^{1/3}$	$c_3 = 2.9$	Koh (1966)
	in $T_s \sim N^{-1}Gr^4Sc^3$		

TABLE 1. Flow regimes for axisymmetric withdrawal from a continuously stratified fluid. The parameters are $S = (Q^2N/\nu^2)^{1/3} = (F^2Gr^4)^{1/3}$, $F = Q/NL^3$, $Gr = N^2L^4/\nu^2$ and $Sc = \nu/D$. From the experiments discussed in §4, $S_{crit} \approx 3$.

diffusion of species becomes important and the flow moves into a viscous-diffusive regime with thickness $\delta \sim (\nu D)^{1/3}L^{1/3}N^{-1/3}$. In this case with S small, viscous forces are important *throughout* the flow field.

These arguments clearly indicate that the parameter S is of importance in determining whether an inertial or a viscous regime is present in the flow field. This parameter should have a value at transition of $S_{crit} \sim 1$, and enables the delineation of a number of possible regimes, each with their own evolution timescales and steady-state thicknesses. Section 4 examines these various regimes in a series of laboratory experiments for a range of values of the parameter S . In anticipation of these data, however, table 1 summarizes the results for axisymmetric withdrawal from a continuously stratified fluid where all scales have been presented in terms of the regime parameter S .

4. Laboratory experiments

4.1. Inertial-buoyancy withdrawal layers

There have been relatively few quantitative laboratory studies on axisymmetric selective withdrawal from continuously stratified fluids. All studies have been in the inertial-buoyancy regime. Lawrence & Imberger (1979) (see also Lawrence 1980) conducted an initial experiment in a long rectangular tank, of width B , with withdrawal from a vertical pipe in the centre of the tank. In a more extensive set of experiments, Spigel & Farrant (1984) also used a relatively long rectangular tank, but there withdrawal was through a circular orifice in one vertical endwall. In both

Experiment	Q (cm ³ /s)	N (rad/s)	ν (cm ² /s)	D (cm ² /s)	$S = \left(\frac{Q^2 N}{\nu^3}\right)^{1/4}$
1	11.8	0.53	1.01×10^{-2}	1.3×10^{-5}	3.35
2	24.3	0.47	1.01×10^{-2}	1.3×10^{-5}	3.65
3	45.2	1.76	1.07×10^{-2}	1.3×10^{-5}	4.28
4	64.6	0.48	1.01×10^{-2}	1.3×10^{-5}	4.16
5	0.14	0.47	0.90×10^{-2}	1.3×10^{-5}	1.88
6	0.21	0.47	0.90×10^{-2}	1.3×10^{-5}	1.98
7	0.47	0.52	0.112	$\approx 8 \times 10^{-7}$	1.34
8	0.84	0.42	0.110	$\approx 8 \times 10^{-7}$	1.64
9	2.33	0.42	0.110	$\approx 8 \times 10^{-7}$	1.64

TABLE 2. Summary of the laboratory experiments on axisymmetric selective withdrawal

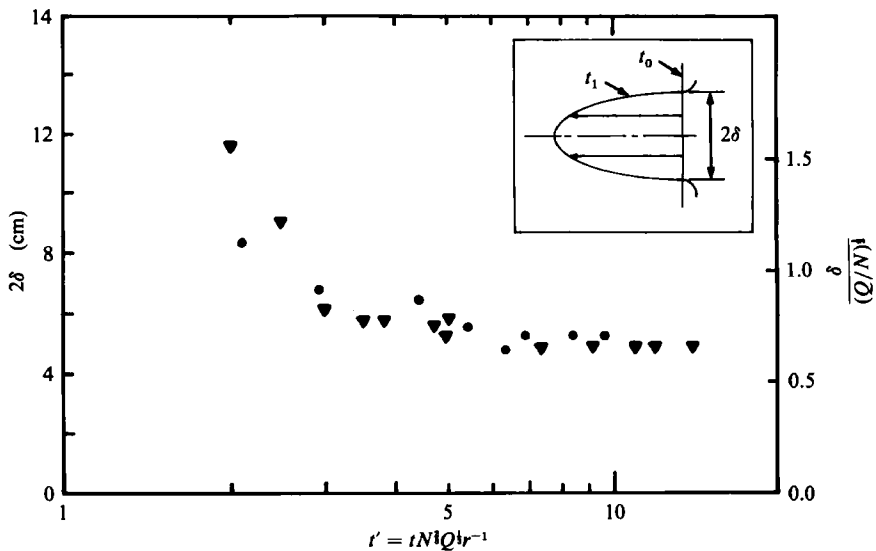


FIGURE 2. Temporal evolution of the withdrawal layer at two locations upstream for an inertial–buoyancy withdrawal layer for experiment 2: ●, $r = 7.5$ cm; ▼, 13.5 cm. The inset sketch illustrates the method of determination of withdrawal-layer thickness from photographs of the distortion of the same dye streak at times $t = t_0$ and $t = t_1$ ($t_1 > t_0$).

cases, the flow towards the sink was radial only for distances upstream of the order of the tank width B . Further upstream, the sidewalls confined the flow, and it was then two-dimensional with an effective discharge per unit width of $q = Q/B$. In all their experiments, however, a virtual control point existed in the radial portion of the flow field since $r_v \sim (Q/N)^{1/2} < B$ in every run. The withdrawal-layer thickness was then determined by the dynamics of the flow in the radial region and influenced by the virtual control point. As a consequence, even though all their measurements were made at distances upstream greater than B , both studies found the withdrawal layer to be of constant thickness and scaled as $\delta \sim (Q/N)^{1/2}$.

It is clear from the discussion in §3 that this result, in turn, has important consequences in delineating the various flow regimes. As a consequence, we decided to conduct additional experiments in this regime, not only over a different parameter range from that of the previous work, but also in a configuration that approached the axisymmetric conditions considered in §3.

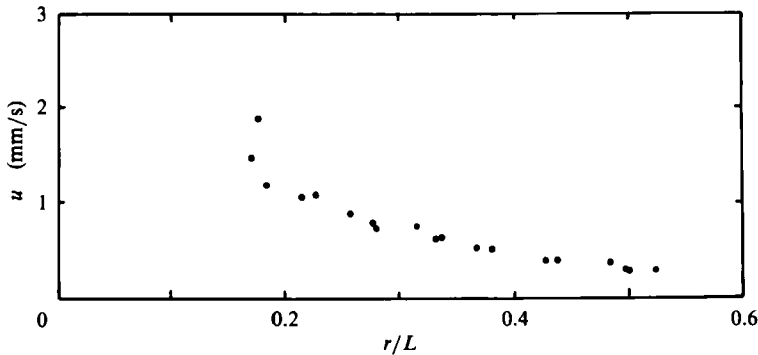


FIGURE 3. Centreline horizontal velocity as a function of radial distance from the sink for experiment 2, at steady-state conditions. Each point is computed by following a single dye trace over time t_0 to t_1 , where the trace has moved correspondingly toward the sink from r_0 to r_1 . The flow is considered steady only if $t > 4N^{-\frac{1}{3}}Q^{-\frac{1}{3}}r$, and the velocity is assumed representative of the location $\frac{1}{2}(r_1 + r_0)$ (where $(r_0 - r_1)/L < 0.06$ in all cases).

All experiments in this study were conducted in a glass tank 60 cm square and 30 cm deep. The tank was filled with a linear density gradient by the two-tank filling technique, using salt as the stratifying medium. The density gradient was then computed from density measurements made with an Anton Paar digital densimeter. The stratifying fluid was either water or a 66% mixture of glycerol and water. In the latter case, all viscosities were measured with Cannon–Fenske tube viscometers and the diffusivity of the stratifying species estimated from Mullin (1971, p. 68). The fluid was withdrawn from the tank via a pipe, of inside diameter 0.4 cm, projecting through the centre of the bottom of the tank and positioned to withdraw from the mid-depth.

The flow was driven by either a gravity feed or, more commonly, a small pump. The withdrawal layer was observed by photographing the distortion over time of dye streaks produced by dropping crystals of Rhodamine B into the tank. The withdrawal-layer thickness δ , in effect the half-thickness, was then determined from the induced velocity field and was taken as the vertical distance from the horizontal centreline of the induced velocity profile to the first zero-crossing, as defined by successive photographs of the same dye streak (see the definition sketch inset in figure 2 above). A number of dye streaks were introduced into the tank, so that the temporal and spatial structure of the withdrawal layer could be examined.

The parameters for the various withdrawal experiments are summarized in table 2. A typical temporal evolution of the withdrawal layer is shown in figure 2, where the total layer thickness is plotted against dimensionless time from table 1. The figure illustrates the asymptotic collapse of the withdrawal layer to the final steady-state withdrawal layer, with thickness independent of distance. The figure suggests that steady state is achieved in times $t \approx 4(N^{-\frac{2}{3}}Q^{-\frac{1}{3}}L)$. Spigel & Farrant (1984) suggested that the time to steady state was $t \approx 2(N^{-\frac{2}{3}}Q^{-\frac{1}{3}}L)$, and both studies are clearly consistent with the anticipated time T_s to steady state in table 2. Figure 3 depicts the steady-state centreline velocity towards the sink: it exhibits a rapid nonlinear decrease in magnitude with increasing radius, as suggested by (5). Taking our slightly more conservative estimate of the time to steady state as representative (i.e. $t = 4T_s$), figure 4 shows the observed steady-state withdrawal-layer thickness for experiments 1–4, all with the regime parameter $S > 3$. The straight line is Lawrence & Imberger's

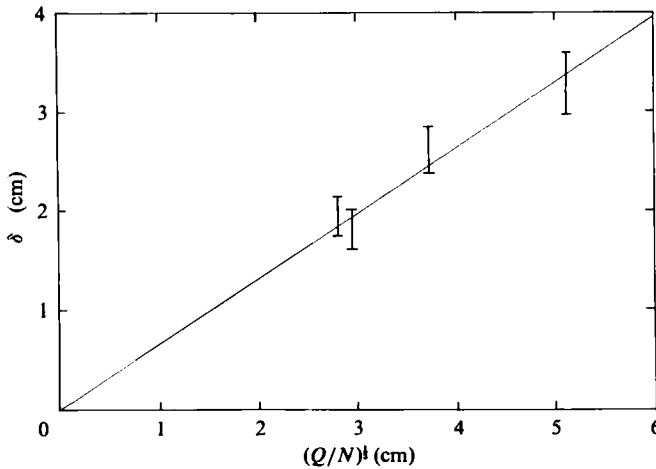


FIGURE 4. Observed steady-state withdrawal-layer thicknesses for experiments 1–4 as a function of the scaled estimate of layer thickness for regime (A) in table 1 (a). The error bars represent plus or minus one standard deviation based on several estimates of layer thickness at different locations and times after steady state.

(1979) suggested correlation of $\delta = 0.66(Q/N)^{1/2}$ for their experiment with $S = 5.12$. Spigel & Farrant found $\delta = 0.81(Q/N)^{1/2}$ as a best fit to their experiments. Clearly the differences between the experiments are slight, and all three studies are in good agreement. They suggest that the layer is inertial–buoyancy for $S > 3$, it reaches steady state in the predicted timescale, it is constant in thickness with distance upstream, and the best estimate of steady-state withdrawal-layer thickness is $\delta = 0.71(Q/N)^{1/2}$ (table 1).

4.2. Viscous–buoyancy withdrawal layers

The analysis of §3 identified a viscous–convective regime (regime C in table 1 b) with an expected steady-state layer thickness of $\delta \sim (\nu Q/N^2)^{1/2}$ and time to steady state $T_s = O(N^{-1}Gr^4S^{-6})$. Using the same laboratory techniques described in §4.1 to estimate withdrawal-layer thickness, figure 5 depicts the temporal evolution of the withdrawal layer for experiment 9, with time non-dimensionalized by this estimate of T_s . In such a viscous fluid ($\nu = 0.11 \text{ cm}^2/\text{s}$ for experiment 9) the primary collapse (in time $T \sim N^{-1}Gr^4$) occurs very rapidly ($t' \approx 0.086$ in the non-dimensionalized timescale of figure 5), and thus with the dye-streak technique it is only practicable to examine the secondary collapse in time $T_s = O(N^{-1}Gr^4S^{-6})$. The data exhibit some scatter, but indicate that the layer approaches steady state in time $t \approx 3T_s$ and has a thickness independent of distance from the sink. Taking the time to steady state as $t = 3T_s$, figure 6 shows the plot of observed steady-state layer thickness for experiments 5–9, where the regime parameter $S < 2$. There is some scatter in the data due (as in figure 5) to the difficulties in making accurate measurements of layer thicknesses from the dye streaks for such very slow flows. Nevertheless, these data indicate the layer is viscous–convective if $S < 2$, the layers collapse to steady state in the expected timescale, and figure 6 suggests that $\delta = 2.1(\nu Q/N^2)^{1/2}$ is a good description of the results. The experiments discussed in §4.1 and in the present section thus suggest that the critical value of S at transition is in the range $S_{\text{crit}} \approx 2\text{--}3$.

Nothing has been said to date about the viscous–diffusive buoyancy layer with a thickness $\delta \sim (\nu D)^{1/2}L^{1/2}N^{-1/2}$ at steady state. It is very difficult to access this regime in

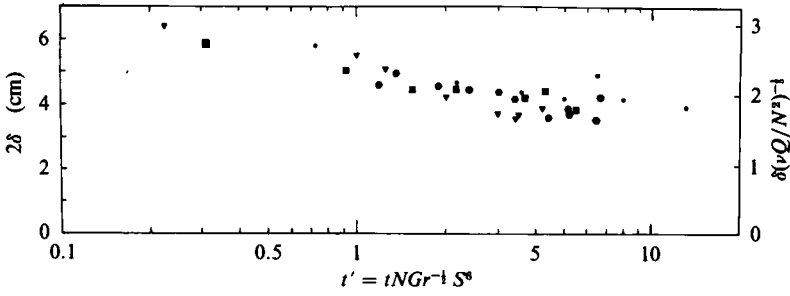


FIGURE 5. Temporal evolution of the withdrawal layer for the viscous-convective regime for experiment 9: ●, $r = 9.5$; ■, 14.5; ◆, 19.5; ▼, 24.0 cm.

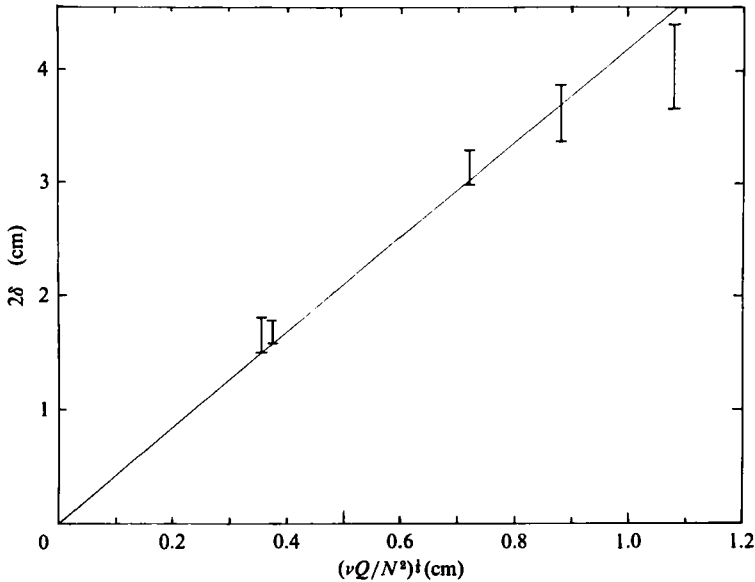


FIGURE 6. Observed steady-state withdrawal-layer thicknesses for experiments 5-9 as a function of the scaled estimate of layer thickness for regime (C) in table 1(b). The error bars indicate one standard deviation about the mean from several estimates of layer thickness at different locations and times after steady state.

the laboratory, and, to our knowledge, no experiments have been made. At steady state this regime has been examined numerically by Koh (1966), however, and from his work $\delta = 2.9(\nu D)^{1/2}L^{1/2}N^{-1/4}$. The results of prior work and the present laboratory experiments are summarized in table 1.

5. Withdrawal from discontinuously stratified fluids

A problem closely related to the withdrawal of fluid from a continuously stratified fluid is that of withdrawal from a fluid with a layered density structure (figure 7). The question of interest is: for a given discharge Q through the point sink and given density stratification, with strength parameterized by $g' = g\Delta\rho/\rho_0$, at what value of lower layer depth d will the upper layer be drawn down? Prior to drawdown the withdrawn fluid comes entirely from the lower layer; after drawdown, it is a mix of

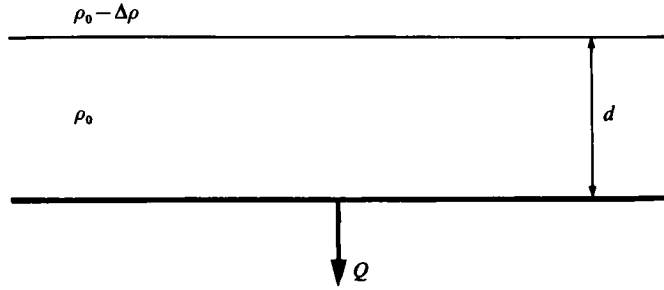


FIGURE 7. Definition sketch of withdrawal from a fluid with a layered density structure.

both layers. For the purpose of our scaling arguments this two-layer stratification may be treated as simply a special case of the linear-stratification problem. The appropriate scales for the critical drawdown conditions may be written down immediately from the results derived in §3.

For the case of the two-layer stratification and in the absence of viscous effects, the critical drawdown condition is achieved when buoyancy and inertia forces are in balance. Since flow is still entirely from the lower layer, the characteristic vertical scale of the motion is d . In the linear-stratification problem we found that when buoyancy and inertia forces were in balance the characteristic vertical scale of the motion was $\delta \sim (Q/N)^{\frac{1}{2}}$ (11). This comparison suggests an analogy between the linear- and two-layer-stratification problems where $\delta \sim d$ and $N^2 \sim g'/d$. Thus, by substituting these scale estimates into (11), we find that critical drawdown occurs when $d \sim (Q^2/g')^{\frac{1}{2}}$. This result, first predicted by Craya (1949) using a rather different approach, was confirmed in experiments by Gariel (1949) and Harleman, Morgan & Purple (1959). Subsequent work (Jirka & Katavola 1979; Blake & Ivey 1985) has shown that the finite size of the outlet can also have an influence on the value of the constant of proportionality in the expression for drawdown height. As in the corresponding regime for continuously stratified fluids, this result implies that at the critical drawdown condition the flow is controlled by a virtual control point upstream from the sink at $r_v \sim (Q^2/g')^{\frac{1}{2}}$, where the local value of the internal Froude number $F_1 = Q(g'd^3)^{-\frac{1}{2}} \sim 1$.

In the case of a linear stratification it was shown in §3.1 that, when viscous effects are important ($R = FG\tau^{\frac{1}{2}} < 1$), an initial or primary withdrawal layer of thickness $\delta \sim (\nu L/N)^{\frac{1}{2}}$ will form in time $T \sim N^{-1}Gr^{\frac{1}{2}}$. Furthermore, in the case of large Sc this layer will subsequently undergo a secondary collapse, and if $Sc^{-\frac{1}{2}} < R < 1$ a layer of thickness $\delta \sim (\nu Q/N^2)^{\frac{1}{2}}$ will form in time $T \sim N^{-1}Gr^{\frac{1}{2}}R^{-\frac{1}{2}}$ (9a). For the case of an infinitely large Sc it is clear that for this secondary collapse $0 < R < 1$, and this result in turn implies the secondary collapse occurs in time $T \sim N^{-1}Gr^{\frac{1}{2}}$ – the formation time of the primary withdrawal layer. Thus for infinitely large Sc for times $T \sim N^{-1}Gr^{\frac{1}{2}}$ a withdrawal-layer structure will have formed with a thickness $\delta \sim (\nu Q/N^2)^{\frac{1}{2}}$.

A discretely layered density stratification is, by definition, non-diffusive or, equally, has an infinitely large Sc . In this limit, for the linear-stratification problem, we see from the above that the only possible withdrawal-layer thickness is $\delta \sim (\nu Q/N^2)^{\frac{1}{2}}$. Again, substituting $N^2 \sim g'/d$ and d for δ , we obtain a second expression for drawdown height $d \sim (\nu Q/g')^{\frac{1}{2}}$, where ν is the viscosity of the layer adjacent to the sink – expressing the fact that buoyancy and viscous forces are now in balance at the critical drawdown condition. Blake & Ivey (1985) conducted a series of laboratory experiments in viscous fluids and confirmed this predicted drawdown height.

Regime	Drawdown height	Constant of proportionality	Source
$S > S_{crit}$	$d = c_1 \left(\frac{Q^2}{g'}\right)^{\frac{1}{2}}$	$c_1 = 0.69\uparrow$ $c_1 = 0.81\ddagger$	Craya (1949) Harleman <i>et al.</i> (1959)
$S < S_{crit}$	$d = c_2 \left(\frac{\nu Q}{g'}\right)^{\frac{1}{2}}$	$c_2 = 2.1$	Blake & Ivey (1985)

† Theoretical value for a point sink.
 ‡ Experimental value for sink of finite size (see text).

TABLE 3. Axisymmetric drawdown (drawup) heights from a layered density structure, where $S = (Q^3g'/\nu^5)^{\frac{1}{2}}$ and $S_{crit} \approx 2-5$

To distinguish between these two possibilities we follow the procedure used in deriving (12) and simply match the two scales. This yields the transition criterion $S = (Q^3g'/\nu^5)^{\frac{1}{2}}$. When S is large inertial forces dominate, and for small S viscous forces are important. The results of Blake & Ivey (1985) suggest that the value of the transition between the two regimes actually occurs for S over the range 2–5, depending upon the importance of finite pipe diameter and interfacial thickness. Table 3 summarizes the possible regimes and the predicted critical drawdown (or drawup) heights in a layered stratification.

6. Inflow

6.1. Inflow into a continuously stratified environment

The axisymmetric inflow of a homogeneous fluid into a stratified container may be treated in similar fashion to the analysis in §3 above. Attention is focused here on the case of a neutrally buoyant inflow at constant discharge Q with low momentum such that there are no entrance mixing effects. As ITF first pointed out, exact symmetry exists between the scaling of the inflow and outflow problems. The same flow regimes as in §3 may be identified.

If the parameter S is large, viscosity is unimportant and the thickness of the inflow is $\delta \sim (Q/N)^{\frac{1}{2}}$ from table 1 (a). For a spreading axisymmetric inflow, conservation of mass requires

$$Qt \sim l_r^2 \delta, \tag{13}$$

where l_r is the radial extent of the spreading intrusion. Substituting for δ , we obtain the spreading law

$$l_r \sim (QN^{\frac{1}{2}})^{\frac{1}{2}} t^{\frac{1}{2}}. \tag{14}$$

As for the corresponding inertial-withdrawal problem in §3.2, the implication is that the flow is influenced by a virtual control point at $r_v \sim (Q/N)^{\frac{1}{2}}$.

At large distances from the source, diffusion of species will become important. From table 1 (a) this occurs when $S \sim (GrSc^{-2})^{\frac{1}{2}}$ (i.e. $l_r \sim Q/(\nu D)^{\frac{1}{2}}$), and with $\delta \sim (\nu D)^{\frac{1}{2}} l_r^{-1} N^{-\frac{1}{2}}$ we obtain from (13) the spreading law

$$l_r \sim \left[\frac{Q^3 N}{(\nu D)^{\frac{1}{2}}} \right]^{\frac{1}{2}} t^{\frac{1}{2}}. \tag{15}$$

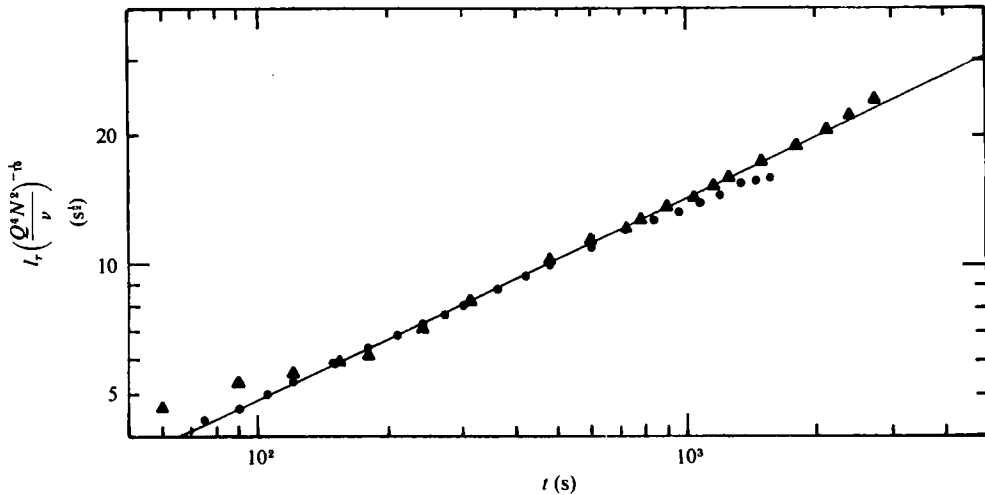


FIGURE 8. Non-dimensionalized spreading radius (from (16)), as a function of time for the experiments on intrusion into a stratified fluid ($Q = 4Q^*$, where Q^* is measured inflow into a 90° sector).

Experiment		Q (cm ³ /s)	N (rad/s)	ν (cm ² /s)	S
1	▲	1.52	0.49	1.00×10^{-2}	2.53
2	●	3.46	1.76	1.06×10^{-2}	3.04

On the other hand, if S is small then viscous forces are important throughout the flow field, from table 1 (*b*) the initial intrusion thickness is $\delta \sim (\nu Q/N^2)^{1/2}$, and we obtain from (13) the spreading law

$$l_r \sim \left(\frac{Q^4 N^2}{\nu} \right)^{1/5} t^{1/2} \quad (16)$$

As in the corresponding withdrawal problem, at large distances from the source, diffusion of species will also become important. From table 1 (*b*) this occurs when $S \sim (GrSc^{-2})^{1/5}$ (i.e. $l_r \sim Q^3 \nu^{1/5} N^{-1/5} D^{-1/2}$), and subsequently the intrusion spreads according to (15).

Of these three possible spreading laws, only the viscous-convective spreading in (16) has been studied. Chen (1980) obtained the result in (16), and used a similarity technique to evaluate the constant of proportionality for the steady state flow. Zatspein & Shapiro (1982) conducted a number of laboratory experiments in the same flow regime, and found good agreement with the predicted spreading law. Unfortunately they do not provide the parameters for all their experiments, although from the limited information provided it seems that the maxima value of S was about 2.7.

Accordingly, we conducted two inflow experiments at the upper end of their experimental range. The same tank and filling system were used as described in §4. The inflow was introduced from a constant-head bucket through a 90° diffuser (radius 3 cm) placed in one corner of the tank. The spreading intrusion was photographed from above, and the results are shown in figure 8, where a best-fit straight line is drawn through the data. For experiment 1 the data for very small time do not collapse onto the line, and this may be due partially to the small but finite size of the diffuser, but it is most likely a result of experimental difficulties in accurately controlling the discharge at such very low flow rates. For a very long time the data in experiment

Regime	Spreading law	Constant of proportionality	Source
$S > (GrSc^{-2})^{\frac{1}{2}}$	$l_r = c_1(QN)^{\frac{1}{2}} t^{\frac{1}{2}}$	(a) $S > S_{crit}$	No data
		$S_{crit} < S < (GrSc^{-2})^{\frac{1}{2}}$	No data
$(GrSc^{-2})^{\frac{1}{2}} < S < S_{crit}$	$l_r = c_3 \left(\frac{Q^4 N^2}{\nu} \right)^{\frac{1}{2}} t^{\frac{1}{2}}$	(b) $S < S_{crit}$	$c_3 = 0.45$ Chen (1980)
			$c_3 = 0.53$ Zatsepin & Shapiro (1982)
			$c_3 = 0.45$ Present study
			average $c_3 = 0.51$
$S < (GrSc^{-2})^{\frac{1}{2}}$	$l_r = c_2 \left[\frac{Q^3 N}{(\nu D)^{\frac{1}{2}}} \right]^{\frac{1}{2}} t^{\frac{1}{2}}$	No data	

TABLE 4. Spreading laws for a homogeneous intrusion into a stratified environment, where $S = (Q^2 N / \nu^3)^{\frac{1}{2}}$

2 start to roll-off the straight line. This roll-off for $l_r/L > 0.6$, where L is the tank length of 60 cm, is an effect of the endwalls and is commonly observed in inflow experiments (e.g. Maxworthy 1972). (For experiment 1 the experiment was terminated when $l_r/L = 0.6$.) The remaining points are well correlated, and the best-fit line indicates that the spreading law is

$$l_r = 0.45 \left(\frac{Q^4 N^2}{\nu} \right)^{0.1} t^{0.48}.$$

These results suggest that the inflow is in this regime for $S < 3$, and the data are in good agreement with the expected spreading law in (16).

The viscous-diffusive spreading law, given by (15), apparently has not been considered by previous investigators. As Ivey & Imberger (1978) found, however, in oceanic or limnological applications the effect of turbulent motions is to change the effective value of the Schmidt number from the molecular value. This change, in turn, may promote a transition to this regime, and thus the relative importance of this spreading law should not be overlooked. As for the corresponding withdrawal flow, it is difficult to access this regime in the laboratory, and it remains uninvestigated.

In addition to the viscous regime in (16), Chen (1980) also argued that an inertial-buoyancy regime existed, which, at steady state, had a spreading law given by

$$l_r \sim (NQ)^{\frac{1}{2}} t^{\frac{1}{2}}. \tag{17}$$

Furthermore, an intrusion that initially obeyed this law would eventually slow until viscous forces became important, at a lengthscale $l_r \sim (Q^3 / N \nu^2)^{\frac{1}{2}}$ (i.e. where $R = FGr^{\frac{1}{2}} \sim 1$ as defined in §3.1). Chen then argues the subsequent spread of the intrusion is described by (16). No experimental evidence is available to confirm the prediction in (17). However, the spreading law in (17) is for an intrusion with a thickness $\delta \sim (Q/Nl_r)^{\frac{1}{2}}$. This is precisely the thickness of the withdrawal layer found in (10c) – a withdrawal-layer thickness that we found was not physically observed, owing to the influence of a virtual control point in the flow (§3.2).

Without experimental evidence it is not possible to differentiate between these two possible spreading laws for inertial inflows. Nevertheless, ITF demonstrated that there was a complete analogy between the outflow and inflow problems in the

case of a line sink or source respectively. Assuming that the same analogy applies for the axisymmetric problem (and it certainly does for viscously dominated flows), between the *observed* axisymmetric withdrawal-layer flows and the corresponding inflows, then (14)–(16) describe the expected spreading behaviour for axisymmetric intrusions into a linearly stratified environment. A summary of the possible laws is given in table 4.

6.2. Inflow of a dense fluid into a homogeneous environment

The axisymmetric spread of a relatively dense (or light) fluid into a homogeneous environment is a problem of some interest. Using the spreading laws for inflows into continuously stratified environments delineated by ITF and the scaled estimate of the density stratification of $N^2 \sim g'/d$ (as in §5), it is straightforward to derive the spreading laws for two-dimensional gravity currents. These spreading laws or regimes and the transition criterion between regimes agree with the independent arguments and experimental observations summarized by Chen (1980). These results suggest the same procedure may be applied here and the spreading laws for axisymmetric density currents derived from the results of the previous sections.

Our interest here is in axisymmetric gravity currents that propagate, without significant mixing, into a homogeneous environment – although buoyancy forces are important over the length l_r of the gravity current. The arguments in §§5 and 6.1 suggest that there are two possible spreading regimes, and the transition between the two is determined by the value of the criterion $S = (Q^3 g' / \nu^5)^{1/5}$ – as in §5.

First, if the parameter S is large then viscosity is unimportant, and, again using the scaled estimate $N^2 \sim g'/d$, we note that the thickness of the inflow is $d \sim (Q^2/g')^{1/2}$ (as for the corresponding critical drawdown depth in table 3). Using the expression for conservation of mass in (13), we obtain the spreading law

$$l_r \sim (Q^3 g')^{1/5} t^{2/5}. \quad (18)$$

As in the inertially dominated regime in §6.1, the implication is that the flow is influenced by a virtual control point, now at $r_v \sim (Q^2/g')^{1/2}$.

Secondly, if the parameter S is small then viscous forces are important over the length of the gravity current, the thickness of the inflow is $d \sim (\nu Q/g')^{1/2}$ (as for the corresponding critical drawdown depth in table 3), and we obtain the spreading law:

$$l_r \sim \left(\frac{Q^3 g'}{\nu} \right)^{1/5} t^{2/5}. \quad (19)$$

Chen (1980) has examined this later regime in a numerical study, and Huppert (1982) has performed a series of laboratory experiments in the same regime.

Didden & Maxworthy (1982) have also made a series of laboratory experiments, which they suggested were in this regime. However, the value of the transition parameter S for the experiments, summarized in their table 2, ranges between 5.77 and 6.97. These values are much larger than the critical value of about 3 suggested by the results in §§4, 5 and 6.1. It suggests their experiments should in fact obey the spreading law described by (18). To test this proposition, the data from their figure 9 are replotted in our figure 9 against the spreading law (18). Clearly, there is an excellent collapse of the data. Didden & Maxworthy did not vary the viscosity, however, and all that can really be said is that their data are consistent with (18). The experiments by Huppert, with a value of S of 0.471 and 0.571 (where g replaces g' in the definition of S for his experiments), are clearly in the viscous regime, and

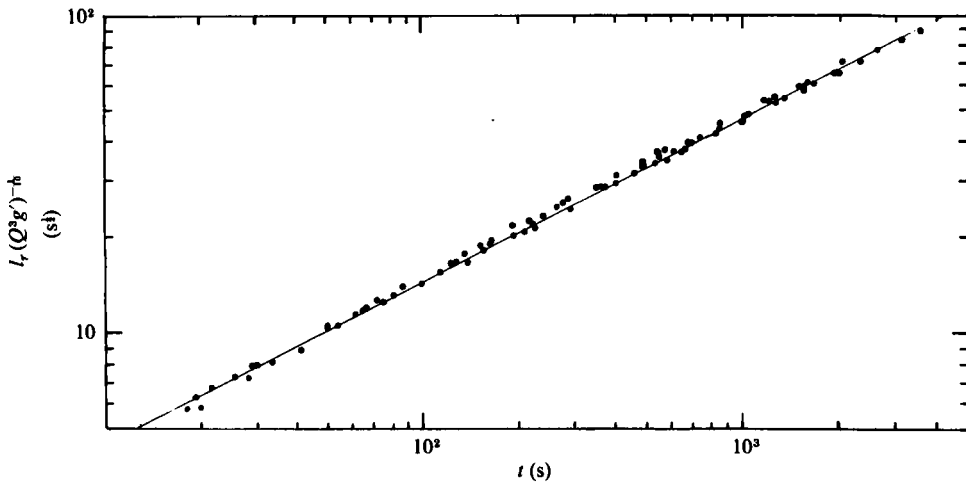


FIGURE 9. Non-dimensionalized spreading radius (from (18)) for the data from Didden & Maxworthy's (1982) figure 9.

Regime	Spreading law	Constant of proportionality	Source
$S > S_{crit}$	$l_r = c_1(Q^2 g')^{1/2} t^{1/2}$	$c_1 = 1.5$	Didden & Maxworthy (1982)
$S < S_{crit}$	$l_r = c_2 \left(\frac{Q^2 g'}{\nu} \right)^{1/2} t^{1/2}$	$c_2 = 0.63$	Chen (1980)
		$c_2 = 0.63$	Huppert (1982)
		average $c_2 = 0.63$	

TABLE 5. Spreading laws for axisymmetric gravity currents, where $S = (Q^2 g' / \nu^2)^{1/2}$

are in close agreement with both Chen's predictions and his own numerical calculations and the predicted spreading law in (19).

Britter (1979) reports a series of laboratory experiments, several runs of which he contends were in the inertial regime. He argues, contrary to (18), the the spreading law is

$$l_r \sim (Qg')^{1/2} t^{1/2} \tag{20}$$

and the inflow thickness $d \sim (Q^2/g'l_r^2)^{1/2}$. This thickness again corresponds to the withdrawal-layer thickness for the continuous-stratification case found in (10c), which was unobtainable owing to the influence of the virtual control point in the flow. Britter (1985, personal communication) has kindly provided his raw data, which are replotted in the Appendix. A close examination of the data reveals that they support neither (20) nor (18). It seems possible that the geometry of the inflow device, and possibly mixing effects, may have influenced the experiments although we are unable to provide a definitive explanation of the actual observations (Appendix). The earlier experiments of Sharp (1969a, b), replotted by Chen (1980), suggest a $t^{1/2}$ dependence as opposed to a $t^{3/4}$ spreading law, although mixing effects driven by the momentum of the input fluid seem likely to be important. Laboratory experiments in the inertial regime with no mixing or source-geometry effects are difficult to perform, but clearly further work is required in order to resolve these questions. However, assuming (as in §6.1) that there is a direct analogy with the withdrawal

problem, the above arguments suggest that (18) and (19) are the appropriate spreading laws for axisymmetric density currents, that they are consistent with published experimental data which cover both regimes, and that table 5 summarizes the possible spreading laws.

7. Conclusions

The axisymmetric withdrawal of fluid from a continuously stratified fluid is a flow with a number of possible flow regimes. In the regime where only inertia and buoyancy are important, our results are consistent with previous work in finding a steady-state withdrawal layer of constant thickness independent of distance from the sink. We argue that this flow is influenced by the presence of a virtual control point in the flow field. Consequently, the analogy between the axisymmetric and the previously studied two-dimensional withdrawal-layer flows breaks down in this regime.

This study has also identified a viscous-convective withdrawal layer flow for high-Schmidt-number fluids with a withdrawal-layer thickness independent of distance from the sink, unlike the two-dimensional case. The existence of this regime is confirmed by laboratory experiments. A third regime also exists in which a viscous-diffusive force balance prevails. The results of the present study suggest that the transition parameter $S = (Q^2 N / \nu^3)^{1/5}$ is the appropriate parameter to differentiate between these possible flow regimes. The parameter S can be interpreted as the ratio of the radial lengthscale at which viscous forces may become important to the radial location of the virtual control point. The laboratory experiments indicate that S has a value of approximately 3 at transition between regimes where inertia is important to those where viscosity is important. A summary of the possible flow regimes for the complete range of flow parameters is given in table 1.

It is argued that these results may also be extended to predict the critical drawdown (or drawup) condition from a two-layered stratification. Two critical drawdown conditions are possible: one in which inertia and buoyancy forces are important, and a second in which viscous and buoyancy forces are important. The results are summarized in table 3.

Imberger *et al.* (1976) have demonstrated that there is a complete analogy between withdrawal and non-mixing inflows into a continuously stratified environment in the case of two-dimensional flows. Assuming that the same analogy exists in the axisymmetric case, and using the above results, the spreading laws for axisymmetric inflows into continuously stratified environments may be readily derived. The predicted spreading laws are summarized in table 4. Similarly, the spreading laws for axisymmetric density currents into homogeneous environments may be simply derived (table 5). While these results differ from previous work – in that for continuous inflows the maximum rate of spread is predicted to be proportional to $t^{1/2}$ – most published data for axisymmetric gravity currents are in agreement with our predictions.

The authors would like to thank Jorg Imberger and Stewart Turner for constructive comments on an earlier draft of this work. They would also like to express their appreciation to Rex Britter for kindly supplying both the data and the details of his original experiments.

Experiment	Q (($\times 10^{-3}$) $\text{cm}^3 \text{s}^{-1}$)	g' (cm s^{-2})	$S = \left(\frac{Q^3 g'}{\nu^5}\right)^{1/3}$	initial slope	final slope
1	4.59	11.8	12.7	1.08	0.72
2	0.861	31.4	10.4	0.94	0.65
3	6.31	35.3	14.0	0.94	0.66
4	3.01	41.2	12.7	0.94	0.63
5	2.62	44.1	12.4	0.96	0.65
6	3.12	18.8	12.2	0.94	0.73
7	2.93	78.5	13.0	0.85	0.60
8	0.0215	34.3	5.98	1.15	0.72
9	0.030	46.1	6.38		0.52

TABLE 6. Summary of the available data from the experiments of Britter (1979) (data supplied by Britter 1985 personal communication)

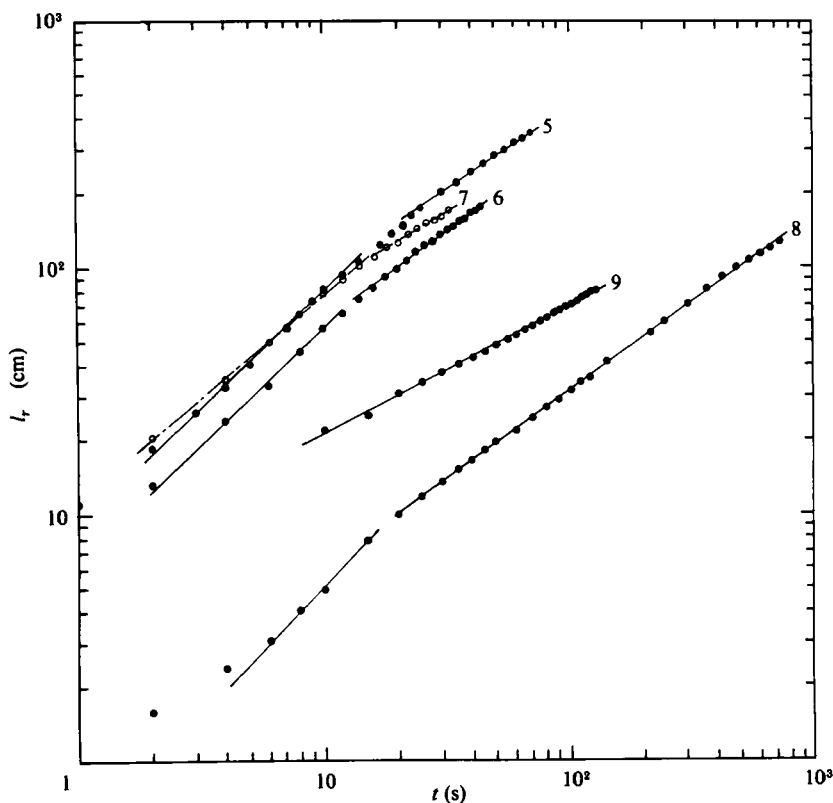


FIGURE 10.

Appendix

Britter (1979) has performed a series of experiments on gravity currents, and has kindly provided the data from his original work. The data from only nine of the original sixteen experiments are now available, and the parameters are summarized in table 6. In order to minimize entrance mixing effects all but one experiment

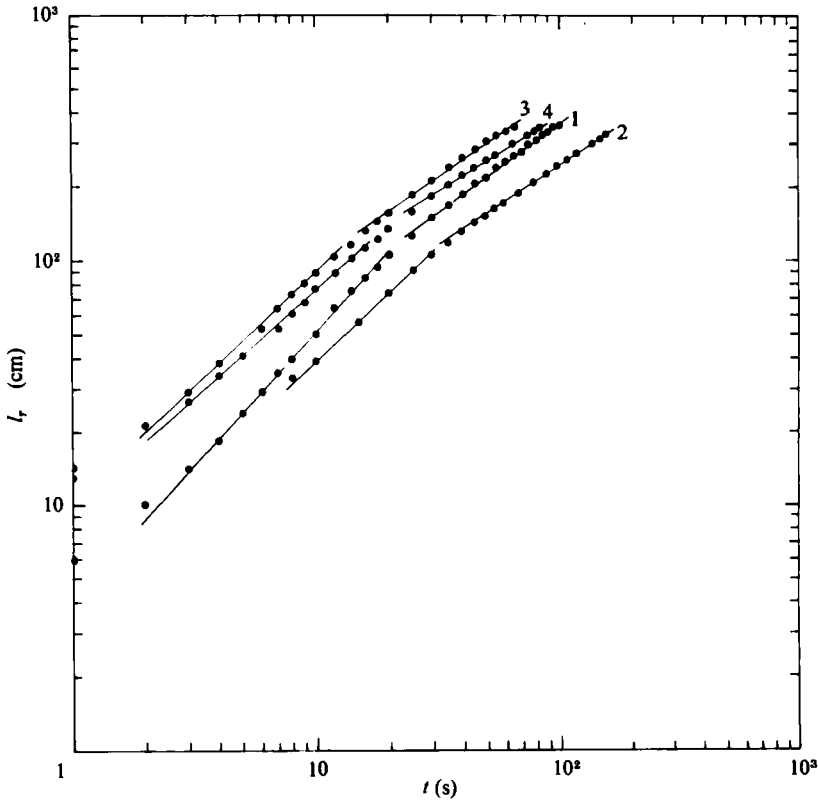


FIGURE 11.

introduced the flow through a 4 cm wide parallel channel, and the flow subsequently emerged into a sector with an included angle of 10° . This necessitated a correction of the space and time origin (such that the density current radius $l_r = 0$ at $t = 0$) and these data, as plotted by Britter (1979) in his figure 2, are replotted here in figures 10 and 11. Two figures are used, for clarity, to illustrate the trends in *each* experiment. For the same reason, experiment 7 in figure 10 is shown plotted with open circles and a dotted best fit by eye.

It is immediately apparent that no one single experiment follows a spreading law proportional to $t^{\frac{1}{2}}$, as predicted by (20). In eight of the runs, the data exhibit a distinct change in slope. The slopes for each of the runs are summarized in the last two columns in table 6. For the first eight runs the average initial slope is 0.98, and the average final slope is 0.67. Run number 9 was performed in the 10° sector without the benefit of the initial 4 cm wide channel section, and exhibits quite a different behaviour ($l_r \propto t^{0.52}$).

The initial slopes of the first eight experiments are close to one, and it is interesting to note that a plane or two-dimensional inertial gravity current will spread at a rate proportional to $t^{1.0}$ (Chen 1980). If the gravity current behaved initially like a two-dimensional current, then one would also expect it to behave more like an axisymmetric gravity current for large radii as it advanced further into the 10° sector. The observed spreading law of $t^{0.67}$ is not predicted, however, by either (18) or (20). While entrance mixing effects were minimized in the experiments, there are some mixing effects at the gravity-current head observed in the experiments. In addition,

there are difficulties associated with defining the space and, in particular, the time origins, and the values assigned to these origins influence the apparent spreading law when the data are plotted. These difficulties conspire to prevent a definitive explanation of the experimental observations by either (18) or (20), and suggest that further experiments could usefully be performed.

REFERENCES

- BLAKE, S. & IVEY, G. N. 1985 Magma mixing and the dynamics of withdrawal from stratified reservoirs. *J. Volcanol. Geotherm. Res.* (to be published).
- BRITTER, R. E. 1979 The spread of a negatively buoyant plume in a calm environment. *Atmos. Environ.* **13**, 1241–1247.
- BRYANT, P. J. & WOOD, I. R. 1976 Selective withdrawal from a layered fluid. *J. Fluid Mech.* **77**, 581–591.
- CHEN, J.-C. 1980 Studies on gravitational spreading currents. *Rep. KH-R-40, Calif. Inst. Tech.*
- CRAYA, A. 1949 Recherches théorétiques sur l'écoulement de couches superposées de fluides de densités différentes. *Houille Blanche* **4**, 44–55.
- DIDDEN, N. & MAXWORTHY, T. 1982 The viscous spreading of plane and axisymmetric gravity currents. *J. Fluid Mech.* **121**, 27–42.
- FASHAM, M. J. R. 1978 The statistical and mathematical analysis of plankton patchiness. *Oceanogr. Mar. Biol. Ann. Rev.* **16**, 43–79.
- GARIEL, P. 1949 Recherches expérimentales sur l'écoulement de couches superposées de fluides de densités différentes. *Houille Blanche* **4**, 56–64.
- HARLEMAN, D. R. F., MORGAN, R. L. & PURPLE, R. A. 1959 Selective withdrawal from a vertically stratified fluid. In *Proc. 8th Congr. IAHR, Montreal*, pp. 10-C-1–10-C-16.
- HUPPERT, H. E. 1982 The propagation of two-dimensional and axisymmetric viscous gravity currents over a rigid horizontal surface. *J. Fluid Mech.* **121**, 43–58.
- IMBERGER, J. 1980 Selective withdrawal: a review. In *Proc. 2nd Intl Symp. on Stratified Flows, Trondheim*, pp. 381–400. Tapir.
- IMBERGER, J., THOMPSON, R. O. R. Y. & FANDRY, C. 1976 Selective withdrawal from a finite rectangular tank. *J. Fluid Mech.* **78**, 489–512.
- IVEY, G. & IMBERGER, J. 1978 Field investigation of selective withdrawal. *J. Hydraul. Div. ASCE* **104**, 1225–1237.
- JIRKA, G. H. & KATALOVA, D. S. 1979 Supercritical withdrawal from two-layered fluid systems, Part 2. Three-dimensional flow into a round intake. *J. Hydraul. Res.* **17**, 53–62.
- KOH, R. C. Y. 1966 Viscous stratified flow towards a sink. *J. Fluid Mech.* **24**, 555–575.
- LAWRENCE, G. A. 1980 Selective withdrawal through a point sink. In *Proc. 2nd Intl Symp. on Stratified Flows, Trondheim*, pp. 411–425. Tapir.
- LAWRENCE, G. A. & IMBERGER, J. 1979 Selective withdrawal through a point sink in a continuously stratified fluid with a pycnocline. *Rep. ED-79-002, Univ. W. Australia*.
- MC EWAN, A. D. & BAINES, P. G. 1974 Shear fronts and an experimental stratified shear flow. *J. Fluid Mech.* **63**, 257–272.
- MAXWORTHY, T. 1972 Experimental and theoretical studies of horizontal jets in a stratified fluid. In *Proc. Intl Symp. on Stratified Flows, Novosibirsk*, pp. 611–618.
- MULLIN, J. W. 1972 *Crystallization*. Butterworth.
- PAO, H. P. & KAO, T. W. 1974 Dynamics of establishment of selective withdrawal of a stratified fluid from a line sink. Part 1. Theory. *J. Fluid Mech.* **65**, 657–688.
- SHARP, J. J. 1969a Spread of buoyant jets at the free surface. *J. Hydraul. Div. ASCE* **95**, 811–825.
- SHARP, J. J. 1969b Spread of buoyant jets at the free surface – II. *J. Hydraul. Div. ASCE* **95**, 1771–1773.
- SPIGEL, R. A. & FARRANT, B. 1984 Selective withdrawal through a point sink and pycnocline formation in a linearly stratified flow. *J. Hydraul. Res.* **22**, 35–51.
- ZATSEPIN, A. G. & SHAPIRO, G. I. 1982 A study of axisymmetric intrusions into a stratified fluid. *Izv. Atmos. Oceanic Phys.* **18**, 77–80.